Synthesis, structure, and ferromagnetism of the oxygen defect pyrochlore system $Lu_2V_2O_{7-x}$ ($x=0.40-0.65$)

G. T. Knoke,* A. Niazi,† J. M. Hill, and D. C. Johnston
Ames Laboratory and Department of Physics and Astronomy, Iowa State University, Ames, Iowa 50011, USA
(Received 24 October 2006; revised manuscript received 16 April 2007; published 21 August 2007)

A fcc oxygen defect pyrochlore structure system $Lu_2V_2O_{7-x}$ with $x=0.40-0.65$ was synthesized from the known fcc ferromagnetic semiconductor pyrochlore compound $Lu_2V_2O_7$ which can be written as $Lu_2V_2O_6O'$ with two inequivalent oxygen sites O and O′. Rietveld x-ray diffraction refinements show significant Lu-V antisite disorder for $x \gtrsim 0.5$. The lattice parameter versus x (including $x=0$) shows a distinct maximum at $x \sim 0.4$. We propose that these observations can be explained if the oxygen defects are on the O′ sublattice of the structure. The magnetic susceptibility versus temperature exhibits Curie-Weiss behavior above 150 K for all x, with a Curie constant C that *increases* with x as expected in an ionic model. However, the magnetization measurements also show that the (ferromagnetic) Weiss temperature θ and the ferromagnetic ordering temperature T_C both strongly *decrease* with increasing x instead of increasing as expected from $C(x)$. The T_C decreases from 73 K for $x=0$ to 21 K for $x=0.65$. Furthermore, the saturation moment at a field of 5.5 T at 5 K is nearly independent of x, with the value expected for a fixed spin 1/2 per V. The latter three observations suggest that $Lu_2V_2O_{7-x}$ may contain localized spin 1/2 vanadium moments in a metallic background that is induced by oxygen defect doping, instead of being a semiconductor as suggested by the $C(x)$ dependence. We present evidence of magnetic granularity in $Lu_2V_2O_{7-x}$ with increasing x, due to the random distribution of oxygen vacancies and associated Lu-V antisite mixing. For $x=0.65$, isothermal magnetization versus magnetic field $M(H)$ and low-field $M(T)$ measurements indicate the formation of interacting nanoscopic ferromagnetic domains below T_C.

DOI: 10.1103/PhysRevB.76.054439 PACS number(s): 75.50.Dd, 75.30.Cr, 61.10.Nz, 61.72.Dd

I. INTRODUCTION

The surprising discovery of heavy fermion behaviors in the metallic fcc normal spinel structure *d*-electron compound LiV_2O_4 at low temperatures $T \lesssim 10$ K (Refs. 1 and 2) illustrates that highly unconventional ground states can accrue to metallic compounds in which geometric frustration for antiferromagnetic ordering is present within a magnetic sublattice of the structure. At high $T \gtrsim 50$ K the V spin $S=1/2$ sublattice interacts antiferromagnetically and consists of corner-sharing tetrahedra with the edges of the tetrahedra running along the six [110] crystal directions. Each V tetrahedron of course consists of triangles for which a collinear antiferromagnetic ordering does not minimize the interaction energy of the sublattice. This geometric frustration has a tendency to suppress static long-range antiferromagnetic ordering, and in the case of LiV_2O_4 probably contributes to the formation at low temperatures of a heavy fermion state instead.

In our search for the same or other interesting ground states of such metallic oxide systems containing frustrated arrays of local magnetic moments, we turned to materials crystallizing in the well-known fcc pyrochlore structure[3] with generic formula $A_2B_2O_7$ in which the interpenetrating A and B sublattices are each identical to the V sublattice in LiV_2O_4.[4] The pyrochlore structure has been very popular and important for the study of geometric magnetic frustration effects, but most such studies have been on insulating rather than metallic systems. There are two crystallographically inequivalent types of oxygen atoms O and O′ in the structure, corresponding to the formula $A_2B_2O_6O'$, as illustrated in Fig. 1 for the known ferromagnetic semiconducting pyrochlore compound $Lu_2V_2O_7$ with a Curie temperature T_C of about 73 K.[5–12] This compound contains V^{+4} d^1 cations with spin $S=1/2$ which give rise to the magnetic ordering (the Lu^{+3} cations are nonmagnetic). Interestingly, the O′ atoms are located at the centers of the Lu^{+3} tetrahedra. The result of this

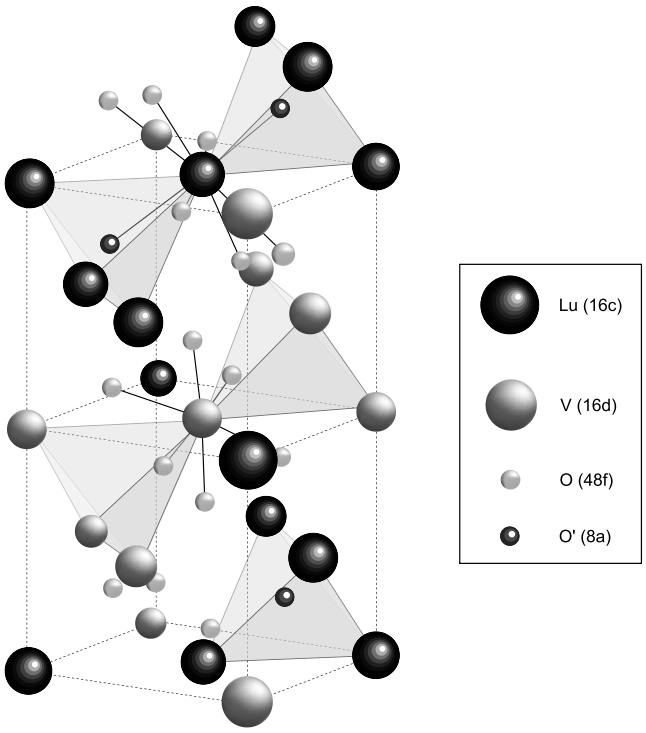

FIG. 1. Pyrochlore crystal structure of $Lu_2V_2O_7$.

is that the Lu site is eightfold coordinated by oxygen as compared to the sixfold coordination of V. Thus in $A_2B_2O_7$ pyrochlore compounds the *A* atom is often a lanthanide atom and the *B* atom is often a transition metal. In the absence of the O′ atoms, both the Lu and V atoms would have been sixfold coordinated by oxygen; this is relevant to our proposed structural model for the oxygen defects in $Lu_2V_2O_{7-x}$ to be introduced later in Sec. II C.

In an attempt to dope the compound $Lu_2V_2O_7$ to induce metallic character, we tried to synthesize the unknown hypothetical compound $Lu_2V_2O_6F$ in which the O′ atom in $Lu_2V_2O_7$ would be completely replaced by F, leading to a crystallographically ordered compound with a nonintegral oxidation state of +3.5 for V as in LiV_2O_4. If the structure remained cubic, that compound would have been metallic by symmetry. Using conventional solid state methods, a clean synthesis was carried out in a sealed Mo crucible at 1250 °C, but unfortunately the product did not crystallize in the pyrochlore structure.

In a further attempt to induce a nonintegral V oxidation state in $Lu_2V_2O_7$, we next tried to create oxygen vacancies that would result in the composition $Lu_2V_2O_{7-x}$; for $x=1/2$, the oxidation state of the V would again be +3.5 as in LiV_2O_4. These efforts were successful as described herein, yielding compounds with $x=0.40-0.65$. Our different types of magnetization data give conflicting indications regarding the metallic character of $Lu_2V_2O_{7-x}$, as will be described. In general, the crystallographic and magnetic properties evolve in interesting and unexpected ways with increasing *x*. Here we report the synthesis, structure, and magnetic properties of the oxygen defect pyrochlore system $Lu_2V_2O_{7-x}$. The synthesis and structural studies are presented in Sec. II, and the magnetization measurements and analyses are in Sec. III. A summary is given in Sec. IV.

II. SYNTHESIS AND STRUCTURE OF $Lu_2V_2O_{7-X}$ ($x=0, 0.40-0.65$)

A. Synthesis

$Lu_2V_2O_7$ was synthesized by calcining pelletized stoichiometric quantities of 99.995% pure (metals basis) Lu_2O_3 (Stanford Materials Corp.), V_2O_3, and V_2O_5 (MV Laboratories, Inc.) in sealed silica tubes at 1250 °C for 72 h with two intermediate grindings. Samples of $Lu_2V_2O_{7-x}$ were subsequently prepared by reducing powdered $Lu_2V_2O_7$ in a mixture of 4.5% H_2 in He at temperatures ranging from 550 to 750 °C, as listed in Table II. If the reduction temperature was increased to 800 °C, x-ray and magnetization data showed that the different compound $LuVO_3$ (see, e.g., Refs. 13 and 14) was obtained instead of pyrochlore structure $Lu_2V_2O_{7-x}$. The most effective method of synthesis was to reduce a sample of $Lu_2V_2O_7$ under flowing H_2 and/or He gas in a Perkin-Elmer Thermogravimetric Analyzer (TGA). Synthesis was regarded as complete when weight loss ceased at a given temperature and the weight remained stable for at least 1 h. The time to completion depended on a combination of factors including the reduction temperature and the amount of sample used. Typical samples (40–50 mg) took approximately two days to stabilize at a reduced composition, and larger samples more than three days. The most homogeneous samples were produced by heating at a ramp rate of 2 °C/min followed by a two-day hold and a subsequent 2 °C/min cooling rate with a 15 min hold after room temperature had been reached to allow the TGA to stabilize. Two series of $Lu_2V_2O_{7-x}$ samples, "gtk-4-11-n" and "gtk-4-5c2-n," were synthesized and studied.

The oxygen content of the parent $Lu_2V_2O_7$ samples was determined via oxidation to V^{+5} in the TGA under O_2. A typical value of the oxygen content was 6.98(7). For the oxygen deficient $Lu_2V_2O_{7-x}$ samples, the weight loss during synthesis in the TGA was used to calculate the oxygen content, assuming the parent compound had exactly $x=0$. Attempts to produce $Lu_2V_2O_{7-x}$ in a tube furnace under flowing H_2 in He were largely unsuccessful. The precise temperature of the sample within the furnace was difficult to measure and it was impossible to know when the reduction had ceased without a constant monitor on the weight. Check-

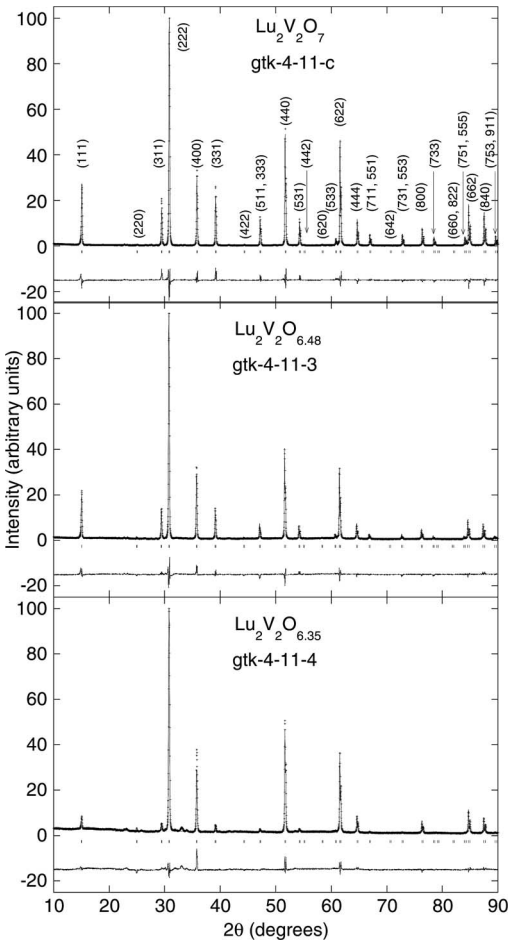

FIG. 2. Indexed x-ray powder diffraction patterns obtained using Cu $K\alpha$ radiation, their Rietveld refinement fits, the expected line positions (ticks), and the differences between observed and calculated intensities, for three single-phase samples of $Lu_2V_2O_{7-x}$ with $x=0.00$, 0.52, and 0.65. The strong decrease in the (odd odd odd) reflection intensities with increasing *x* results from Lu-V antisite disorder. The goodnesses of fit were $R_{wp}=15.0\%$ for $x=0$, $R_{wp}=12.3\%$ for $x=0.52$, and $R_{wp}=11.0\%$ for $x=0.65$. The respective R_{wp}/R_p values are given in Table II.

TABLE I. Crystal data for $Lu_2V_2O_{7-x}$.

Space group	$Fd\bar{3}m$ (227), origin at center ($\bar{3}m$)
Z	8
Atomic positions	Lu, 16(c), ($\bar{3}m$), (0,0,0)
	V, 16(d), ($\bar{3}m$), $(\frac{1}{2},\frac{1}{2},\frac{1}{2})$
	O, 48(f), mm, $(\frac{1}{8},\frac{1}{8},z)$
	O′, 8(f), $43m$, $(\frac{1}{8},\frac{1}{8},\frac{1}{8})$
Wavelength	1.54060 Å
2θ range	5°–110°
Number of reflections	90
Profile function	pseudo-Voigt

ing the weight periodically by removing the sample from the furnace proved disastrous as repeated heating and cooling cycles caused the samples to decompose. These samples had multiple Curie temperatures, were generally of poor quality, and will not be further discussed. In view of these results and the relatively low temperatures (550–750 °C) at which the samples are synthesized compared to the temperature (1250 °C) needed to synthesize the $Lu_2V_2O_7$ parent compound, the oxygen defect system $Lu_2V_2O_{7-x}$ may be metastable.

B. Structure

Powder x-ray diffraction (XRD) patterns were obtained using a Rigaku Geigerflex diffractometer and Cu $K\alpha$ radiation, in the 2θ range from 5° to 110° with a 0.02° step size. Intensity data were accumulated for 5–10 s/step. The small powder sample amounts available ($\lesssim$50 mg, see above) constrained us to mount the powder on vaseline-coated glass microscope slides for XRD specimens. The amorphous vaseline and glass background at low angles restricted subsequent Rietveld refinement of some of the XRD patterns to $2\theta > 20°$. However, the restricted range eliminated only the initial (111) reflection and did not significantly affect the results. A typical sample of $Lu_2V_2O_{7-x}$ showed a single phase x-ray diffraction pattern with lattice parameters similar to those of the parent compound as shown for several samples in Fig. 2. It is important to note that the intensities of the reflections with Miller indices (hkl) all odd become greatly suppressed with increasing oxygen deficiency above $x \approx 0.4$ compared to the reflections with (hkl) all even. This reduction in the (odd, odd, odd) reflection intensities is a very sensitive indicator of antisite disorder between the Lu and V sites of the pyrochlore structure as reported for (Sc,Lu)-V antisite disorder in the system $(Lu_{1-x}Sc_x)_2V_2O_7$.[9] This means that Lu and V atoms switch places to increasing degrees with increasing oxygen deficiency x.

To quantitatively characterize the changes in the structure of $Lu_2V_2O_{7-x}$ with increasing x, Reitveld refinements of the x-ray diffraction data were carried out using the program DBWS9807A.[15] The atomic positions of the atoms in the pyrochlore structure of $Lu_2V_2O_7$ are shown in Table I, together with several parameters associated with the Rietveld refinements. Table I shows that the Lu, V, and O′ positions are all fixed with respect to the unit cell edges, and only the z coordinate of the O position is variable. The initial O z coordinate was taken to be that reported for $Lu_2V_2O_7$ by Soderholm and Greedan.[12] Keeping in mind the limitations of our

TABLE II. Structure parameters for $Lu_2V_2O_{7-x}$ refined from powder XRD data. T_{prep} is the preparation temperature. The overall isotropic thermal parameter B is defined within the temperature factor of the intensity as $e^{-2B\sin^2\theta/\lambda^2}$.

Sample gtk-4-	T_{prep} (°C)	x	a (Å)	z of O at 48(f)	Lu-V disorder	V-O-V (°)	B (Å^2)	R_{wp}/R_p
5-c2	1250	0	9.9368(1)	0.426(1)	0[a]	134.5	0.62(2)	1.30
5-c2-7[b]	550	0.44	9.9721(3)	0.416(1)	0.00(1)	128.9	2.47(4)	1.33
5-c2-5[b]	650	0.52	9.9643(2)	0.409(1)	0.05(1)	125.5	1.92(3)	1.32
5-c2-6	700	0.65	9.9502(3)	0.407(1)	0.25(1)	124.4	2.79(3)	1.36
11-c	1250	0	9.9401(1)	0.427(1)	0[a]	134.8	1.03(2)	1.32
11-1[b]	550	0.40	9.9618(2)	0.419(1)	0.00(1)	130.6	2.94(4)	1.31
11-2[b]	600	0.48	9.9604(3)	0.414(1)	0.03(1)	128.1	3.12(4)	1.37
11-3	650	0.52	9.9560(2)	0.411(1)	0.09(1)	126.7	3.12(3)	1.33
11-5	700	0.58	9.9526(3)	0.406(1)	0.15(1)	123.8	2.73(3)	1.32
11-4	750	0.65	9.9424(3)	0.391(1)	0.30(1)	116.9	2.72(3)	1.28

[a]Rietveld refinement of the XRD data gave small unphysical negative values (≈ -0.01) for the Lu-V antisite disorder, i.e., for site occupancy by the minority species [V at the Lu 16(c) site and Lu at the V 16(d) site]. The antisite disorder was therefore fixed to be zero for subsequent refinements.

[b]Two-phase sample with about 20 mol % or less (from Reitveld refinement of the XRD data) of stoichiometric $Lu_2V_2O_7$. The overall composition x and the refined fraction of the $Lu_2V_2O_{7-x}$ phase in each two-phase sample were 0.35 and 79(2)% for gtk-4-5-c2-7, 0.49 and 95(1)% for gtk-4-5-c2-5, 0.32 and 80(1)% for gtk-4-11-1, and 0.39 and 82(1)% for gtk-4-11-2. The composition and structure parameters reported in the table are for the oxygen defect $Lu_2V_2O_{7-x}$ phase in each sample.

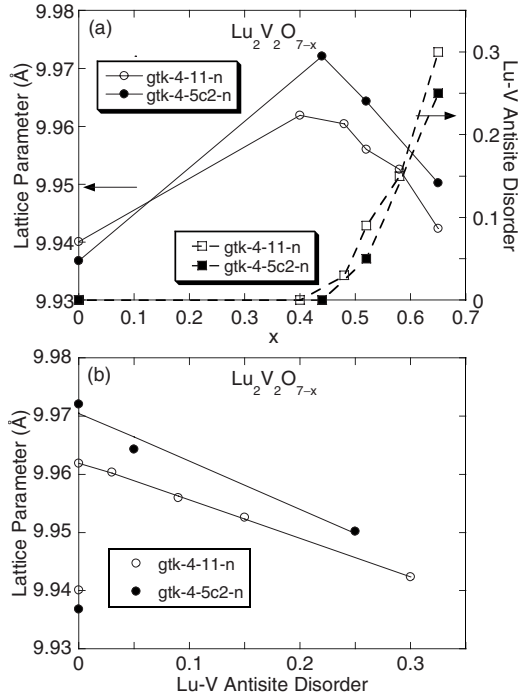

FIG. 3. (a) Refined lattice parameter (left scale) and Lu-V antisite disorder (right scale) as functions of (corrected) x for two series of $Lu_2V_2O_{7-x}$ samples. (b) Refined lattice parameter as a function of the Lu-V antisite disorder. The straight lines are linear fits to the data for $x>0.4$. The error bars are smaller than the size of the data symbols.

XRD data, the TGA results were used to determine the oxygen site occupancy, with the vacancies being ascribed to the O′ site (see the structural model in Sec. II C). Thus we did not refine the oxygen site occupancies. Similarly, the quality of the XRD patterns was such that only an overall isotropic thermal parameter B was refined. Furthermore, the surface roughness was not refined, which can affect the fitted values of B. The parameters refined were B, scale, sample height, sample transparency, background, lattice spacing, the O position z value, pseudo-Voigt profile shape, full width at half maximum, and the Lu-V antisite disorder. The XRD patterns of samples with overall $x<0.5$ showed the presence of stoichiometric $Lu_2V_2O_7$ (~20 mol % or less) in addition to $Lu_2V_2O_{7-x}$, probably due to kinetic limitations during the reduction process, and were refined as two-phase mixtures. The reported structure parameters for $Lu_2V_2O_{7-x}$ are those refined for this phase. Bond lengths and angles were computed from the refined structure parameters using PowderCell for Windows.[16] The XRD refinement parameters are shown in Table II. The Reitveld refinement fits for single phase samples with $x=0$, 0.52, and 0.65 are shown in Fig. 2.

The lattice parameter and Lu-V antisite disorder are plotted as functions of the oxygen deficiency x for the two series of $Lu_2V_2O_{7-x}$ samples in Fig. 3(a). The lattice parameter varies nonmonotically, initially increasing, and then decreasing for increasing x, thus strongly violating Vegard's law. In the absence of samples with $0<x<0.4$ it is not possible to pinpoint the x value corresponding to the maximum in the lattice parameter, but similar behavior was observed for both series of samples. The refined Lu-V antisite disorder in Fig. 3(a) becomes significant for $x\gtrsim 0.5$ and then increases monotonically with increasing x. The lattice parameter decreases approximately linearly with the Lu-V antisite disorder for $x\geqslant 0.4$, as shown in Fig. 3(b).

C. Structural model for oxygen vacancies in $Lu_2V_2O_{7-x}$

Typically, in oxides V^{+3} or V^{+4} cations are sixfold coordinated by oxygen whereas the larger Lu^{+3} cation is often eightfold coordinated, as in the pyrochlore structure of $Lu_2V_2O_7$ itself, although sixfold coordination for Lu also occurs in some oxide compounds. In view of the Lu-V antisite disorder in $Lu_2V_2O_{7-x}$ that increases with increasing x, and of the nonmonotonic variation in the lattice parameter with x, we propose that the oxygen vacancies in $Lu_2V_2O_{7-x}$ occur on the O′ sublattice of the structure, as follows. Since the O′ anions reside at the centers of the Lu tetrahedra in $Lu_2V_2O_7$ as shown in Fig. 1, O′ vacancies would decrease the average coordination number of the Lu sites by O, thus encouraging V atoms to occupy the Lu sites, which requires Lu to switch places with V (antisite disorder) in order to preserve the overall composition. If both of the O′ atoms on either side of a given Lu site were vacant, which would occur with probability x^2, that Lu site would then have sixfold oxygen coordination as preferred by V cations. The antisite disorder in Fig. 3 is seen to increase nonlinearly with x in qualitative agreement with the model. The reason for the abrupt onset of antisite disorder at $x\approx 0.40$ is not understood.

In this model, we propose that the removal of oxygen from the O′ sites at the centers of the Lu tetrahedra causes an initial increase in the lattice parameter with increasing x from $x=0$ to $x=0.32$ in Fig. 3(a). This arises from the resultant removal of the Lu-O′-Lu bonding within the affected Lu_4O' tetrahedra, thus causing the Lu_4 tetrahedra and the overall lattice to expand. However, at larger $x\gtrsim 0.4$, the smaller ionic radius of the Lu^{+3} ion in the sixfold oxygen-coordinated V site, occurring via Lu-V antisite disorder, compared to its ionic radius in the original eightfold coordinated Lu site, evidently leads to the observed lattice contraction. For $x=0.40-0.65$, the lattice parameter decreases approximately linearly by about 0.02 Å with increasing Lu-V antisite disorder as seen in Fig. 3(b). Indeed, this decrease is about the same as expected from the decrease in ionic radius of Lu^{+3} in eightfold (0.977 Å) to sixfold (0.861 Å) coordination by oxygen with increasing Lu-V antisite disorder, where one utilizes the facts that there are 16 Lu cations per unit cell and that the fractional Lu occupation of V sites increases from about 0 to 0.3 over this x range.

III. MAGNETIZATION MEASUREMENTS AND ANALYSES

A. Measurement results I

Magnetization M data were obtained at temperatures T between 1.8 and 300 K over the applied magnetic field H range from 0 to 5.5 T using a Quantum Design superconducting quantum interfere device (SQUID) magnetometer. As shown for representative samples in Fig. 4, the inverse susceptibility of each $Lu_2V_2O_{7-x}$ composition at tempera-

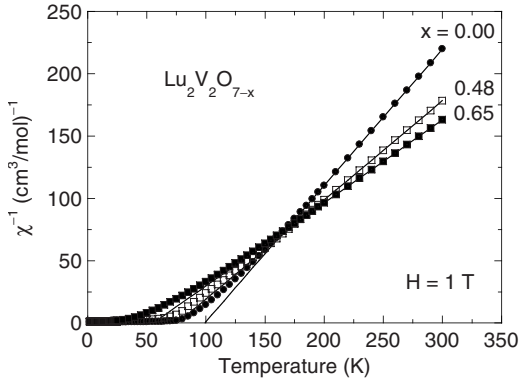

FIG. 4. Inverse of the magnetic susceptibility χ versus temperature in a magnetic field of 1 T for illustrative $Lu_2V_2O_{7-x}$ samples with $x=0$ (sample number gdk-4-5-c2), 0.48 (gdk-4-11-2), and 0.65 (gdk-4-11-4). The Curie-Weiss law fits above 150 K are shown as straight lines and are extrapolated to lower temperatures. The sample with (corrected) $x=0.48$ contains 20(1)% of unreduced $Lu_2V_2O_7$ which has been corrected for in the plotted data.

tures above about 150 K follows the Curie-Weiss law $\chi = C/(T-\theta)$ with Curie constant C and Weiss temperature θ listed in Table III. Representative straight-line fits are shown in Fig. 4.

All $Lu_2V_2O_{7-x}$ samples ($x=0.40-0.65$) exhibited ferromagnetic ordering. The Curie temperatures T_C (Table III) were determined from zero-field-cooled and field-cooled $M(T)$ measurements at a low-field $H=10$ or 20 G, shown in Figs. 5(a) and 5(b) for the gtk-4-11-n series of samples. The straight-line fit to the $M(T)$ data used to determine T_C is exemplified for the $x=0.65$ sample in Fig. 5(c). From Table III, the C and T_C for the two $x=0$ samples are slightly different, possibly due to small differences in the oxygen content of the two samples. The behavior of the field-cooled (fc) $M(T)$ data below T_C for $0.48 \leqslant x \leqslant 0.65$ in Fig. 5 is unusual for a ferromagnet. In particular, the zero-field-cooled (zfc) and fc data *both* show a maximum at a temperature less than or equal to the irreversibility (bifurcation) temperature $T_{\rm irr}$ and decrease at lower temperatures. This interesting effect is investigated and discussed further in Sec. III C.

Isothermal magnetization $M(H)$ curves at $T=5$ K are plotted in Figs. 6(a) and 6(b). The samples with $x \gtrsim 0.5$, containing significant Lu-V antisite disorder, did not completely saturate up to at least $H=5.5$ T. The well-defined saturation moments $\mu_{\rm sat}$ for samples with $x<0.5$ are listed in Table III. Assuming a spectroscopic splitting factor (g factor) $g=2$, the saturation moment of the $x=0$ sample is close to the expected value $\mu_{\rm sat}=gS\mu_B=1\ \mu_B$/V atom, since $S=1/2$ for the V^{+4} cations in that compound. On the other hand, the magnetizatons of all the other samples are also clustered around 1 μ_B/V atom at our highest field of 5.5 T, contrary to expectation (below) that $\mu_{\rm sat}$ should increase with increasing x. $M(H)$ isotherms for sample gtk-4-5-c2-6 with $x=0.65$ at temperatures from 1.8 to 100 K are shown in Fig. 6(c). The data become nonlinear at temperatures significantly above T_C for this sample, which correlates with the high onset temperature of the nonlinear $M(T)$ behavior above T_C in Fig. 4.

The T_C, θ, and C are plotted in Fig. 7(a) versus oxygen deficiency x in $Lu_2V_2O_{7-x}$, where for samples with $x<0.5$ containing unreduced $Lu_2V_2O_7$, the Curie constants and Weiss temperatures have been corrected to reflect the values

TABLE III. Magnetic properties of $Lu_2V_2O_{7-x}$. Here, T_C is the Curie temperature, C the Curie constant, θ the Weiss temperature in the Curie-Weiss behavior of the high-temperature susceptibility, and $\mu_{\rm sat}$ (5 K) the saturation moment at 5 K.

Sample (gtk-)	x	T_C (K)	C (cm^3 K/mol)	θ (K)	$\mu_{\rm sat}$ (5 K) (μ_B/V atom)
4-5-c2	0.00	73.8(1)	0.923(2)	97.4(3)	0.97
4-5-c2-7[a]	0.44	39.0(4)[a]	1.31(2)[a]	72.0(3)[a]	0.95
4-5-c2-5[a]	0.52	35.2(6)[a]	[b]	[b]	[c]
4-5-c2-6	0.65	20.8(2)	[b]	[b]	[c]
4-11-c	0.00	72.0(1)	0.825(1)	97.3(2)	0.95
4-11-1[a]	0.40	37.1(4)[a]	1.20(1)[a]	79.8(5)[a]	0.99
4-11-2[a]	0.48	36.1(12)[a]	1.37(1)[a]	71.5(5)[a]	0.93
4-11-3	0.52	32.2(1)	1.396(1)	66.9(2)	[c]
4-11-5	0.58	27.9(1)	1.457(1)	62.6(1)	[c]
4-11-4	0.65	20.3(2)	1.500(1)	55.4(1)	[c]

[a]This sample shows a second ferromagnetic transition at 73 K indicating a significant fraction of the sample is $Lu_2V_2O_7$ (see Table II). The listed x is the corrected oxygen defect composition of the $Lu_2V_2O_{7-x}$ phase. Since the saturation moment does not significantly depend on the oxygen vacancy composition x in $Lu_2V_2O_{7-x}$, the mixture of $Lu_2V_2O_7$ with $Lu_2V_2O_{7-x}$ does not affect the value of the saturation moment. The observed C and θ values have been corrected so that the listed values correspond to the $Lu_2V_2O_{7-x}$ phase by itself. This was done by correcting the observed susceptibility for that of the relevant amount of the $x=0$ phase and fitting the corrected data above 150 K by a Curie-Weiss law.

[b]The magnetic susceptibility at $H=1$ T was not measured for this sample.

[c]The magnetization of this sample does not completely saturate up to an applied magnetic field $H=5.5$ T.

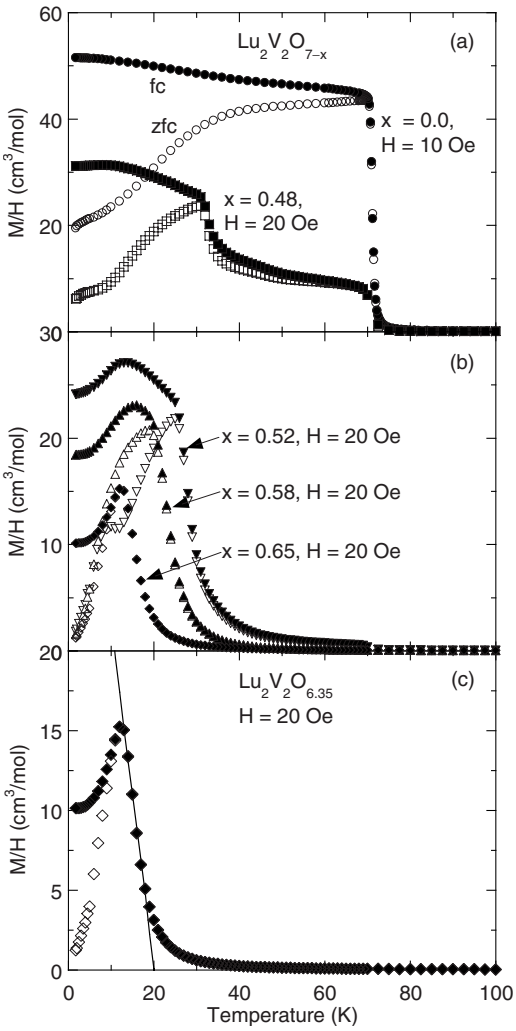

FIG. 5. [(a),(b)] Zero-field-cooled (zfc) (open symbols) and field-cooled (fc) (filled symbols) magnetization versus temperature $M(T)$ data in low magnetic fields H for (corrected) $x=0.0$, 0.48, 0.52, 0.58, and 0.65 of samples from the series gtk-4-11-n. The sample with corrected $x=0.48$ had overall $x=0.39$ and contained 18(2)% of unreduced $Lu_2V_2O_7$, as seen in the corresponding $T_C \approx 73$ K. (c) Expanded plots of the fc and zfc data for the $x=0.65$ sample, showing the straight-line fit to the $M(T)$ data to determine the ferromagnetic ordering temperature T_C.

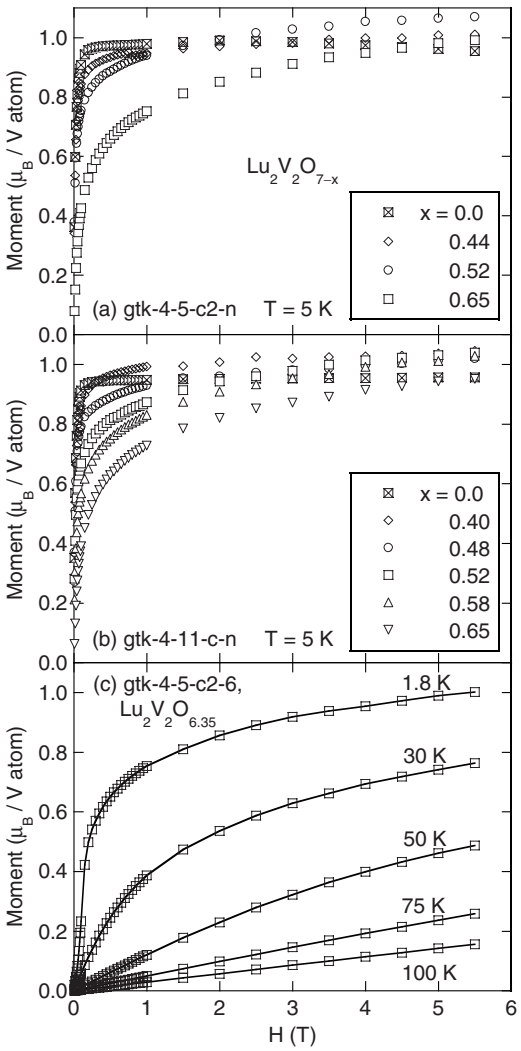

FIG. 6. [(a),(b)] Magnetization versus field at 5 K for the two series of $Lu_2V_2O_{7-x}$ samples gtk-4-5-c2-n and gtk-4-11-n. The samples with $x \gtrsim 0.5$ did not completely saturate up to at least 5.5 T. The samples with listed compositions $x=0.44$ and 0.52 in (a), and $x=0.40$ and 0.48 in (b) contain unreduced $Lu_2V_2O_7$ for which the listed compositions are the actual corrected x values in the oxygen defect phase $Lu_2V_2O_{7-x}$. (c) Magnetization versus field at different temperatures for the $x=0.65$ sample gtk-4-5-c2-6. The nonlinearity in $M(H)$, indicative of short-ranged correlations, persists up to ~75 K, well above $T_C=20.8$ K. The solid lines are guides to the eyes.

of the $Lu_2V_2O_{7-x}$ phase in those three samples. One sees that as the Curie constant C increases, both the Weiss temperature θ and the T_C decrease, contrary to expectation (see below). The θ for each sample is consistently ~30 K higher than T_C, suggesting that T_C is suppressed from the mean-field value $T_C=\theta$ by fluctuation effects.

B. High-temperature magnetic susceptibility data analysis

In the Curie-Weiss law $\chi=C/(T-\theta)$, the Curie constant C of a system of N spins S is expressed as

$$C=\frac{Ng^2S(S+1)\mu_B^2}{3k_B}, \tag{1}$$

where μ_B is the Bohr magneton and k_B is Boltzmann's constant. The Curie-Weiss law is a mean-field expression arising from only nearest-neighbor magnetic interactions and correlations between the spins in the system. For a system containing a random distribution of different spin values S, in mean-field approximation one can replace $S(S+1)$ in Eq. (1) by its average value $\langle S(S+1)\rangle$, i.e.,

$$C=\frac{Ng^2\langle S(S+1)\rangle\mu_B^2}{3k_B}. \tag{2}$$

In $Lu_2V_2O_{7-x}$, the formal oxidation state of the V ions is $4-x$. If the reduction in oxidation state with x does not give rise to itinerant electrons but rather to a random mixture of localized $S=1/2$ (V^{+4}) and $S=1$ (V^{+3}) spins, then in this

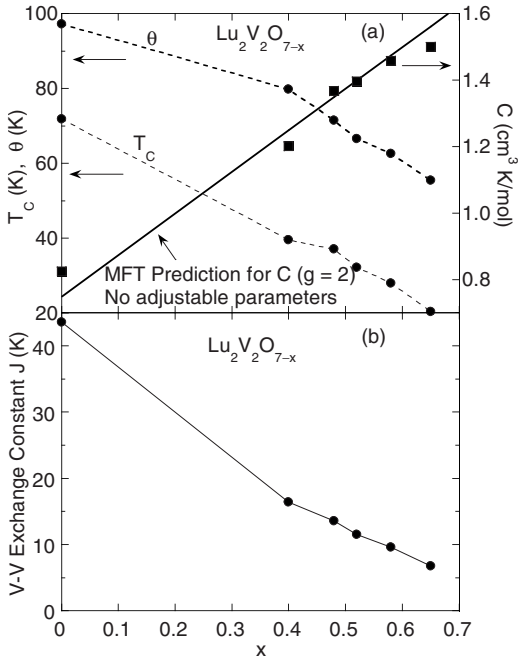

FIG. 7. (a) Curie temperature T_C, Weiss temperature θ (left scale), and Curie constant C (right scale) versus oxygen deficiency x in $Lu_2V_2O_{7-x}$ series gtk-4-11-n. The straight line is the mean-field theory (MFT) prediction for C in Eqs. (4) and (5) assuming a spectroscopic splitting factor $g=2$ for the local magnetic moments in the system, with no (other) adjustable parameters. (b) Variation of the exchange constant J versus composition x in $Lu_2V_2O_{7-x}$, computed using Eq. (10) and the C and T_C data in Table III.

ionic model the probabilities that $S=1/2$ and $S=1$ occur are $p_{1/2}=1-x$ and $p_1=x$, respectively, yielding

$$\langle S(S+1)\rangle = \frac{3+5x}{4}. \tag{3}$$

If the g factors of the spins 1/2 and 1 are the same, one can substitute Eq. (3) into Eq. (2) to obtain the Curie constant as

$$C(x) = C(0)\left(1+\frac{5x}{3}\right), \tag{4}$$

where for $g=2$

$$C(0) = \frac{3}{4}\frac{\text{cm}^3\ \text{K}}{\text{mol}}. \tag{5}$$

Here, a "mol" refers to a mole of $Lu_2V_2O_{7-x}$ formula units containing 2 mole of V atoms. The linear relation with no adjustable parameters in Eqs. (4) and (5) is plotted as the straight line in Fig. 7(a), which describes well the Curie constant data for $x>0$. This agreement suggests that increasing the oxygen vacancy concentration x results in the mixture of localized $S=1/2$ and $S=1$ V spin species dictated by the composition in an ionic model. This in turn suggests that the compound does not exhibit metallic character over our x range. However, one then expects that the saturation magnetic moment $\mu_{\text{sat}}=g\langle S\rangle\mu_B=(1+x)\mu_B$ at $H=5.5$ T should increase with x, instead of remaining nearly independent of x as seen in Table III and Fig. 6.

For a uniform spin S system with the Heisenberg Hamiltonian $\mathcal{H}=-J\Sigma_{\langle ij\rangle}\vec{S}_i\cdot\vec{S}_j$ with nearest-neigbor exchange interaction J, where the sum is over nearest-neighbor spin pairs and $J>0$ corresponds to ferromagnetic coupling, the mean-field ferromagnetic ordering (Curie) temperature is given by

$$T_C = \theta = \frac{zJS(S+1)}{3k_B}, \tag{6}$$

where z is the nearest-neighbor coordination number of a spin with neighboring spins. For a system containing different spin values interacting with the same J for each nearest-neighbor spin pair, the Curie temperature at the mean-field level is then

$$T_C = \frac{zJ\langle S(S+1)\rangle}{3k_B}. \tag{7}$$

Using Eqs. (2) and (7), one can eliminate $\langle S(S+1)\rangle$ and express T_C in terms of C as

$$T_C = \frac{zJC}{Ng^2\mu_B^2}. \tag{8}$$

Thus one expects that as the Curie constant increases with increasing x, T_C should also *increase*. Remarkably, we find instead from Table III and Fig. 7 that both θ and T_C *decrease* with increasing x.

From Eq. (8), one can express J in terms of T_C as

$$J = \frac{Ng^2\mu_B^2 T_C}{zC}. \tag{9}$$

Setting N to be twice Avogadro's number (there are two V atoms per formula unit in $Lu_2V_2O_{7-x}$), $g=2$, $z=6$ from the structure, and taking C from Eqs. (4) and (5), Eq. (9) gives

$$J = 0.500\frac{T_C}{C}, \tag{10}$$

where J and T_C are in units of K and C is in units of cm^3 K/mol. Using Eq. (10) and the $T_C(x)$ and $C(x)$ data in Table III, $J(x)$ was computed and is plotted in Fig. 7(b). One sees that J monotonically and strongly decreases with increasing x, by a remarkable factor of about 6 as x increases from 0 to 0.65.

C. Measurement results II: Ferromagnetic domain granularity below T_{irr} in $Lu_2V_2O_{6.35}$

Figure 5 above shows that the fc and zfc magnetization data in low fields change character below T_C as x increases above (corrected) 0.40. For $x=0$ and $x=0.40$ (not shown for clarity), the fc data increase and the zfc data decrease with decreasing T below the bifurcation temperature (irreversibility temperature T_{irr}) between them, as normally observed for ferromagnets. However, for samples with $x\geqslant 0.48$, the zfc and fc data *both* show a maximum at a $T\leqslant T_{\text{irr}}$ and decrease at lower temperatures, from which one might infer that these compositions are antiferromagnetic rather than ferromagnetic. On the other hand, it is clear from the ferromagnetic

Weiss temperatures in the high-temperature Curie-Weiss susceptibilities of all samples that the dominant interactions in all samples are ferromagnetic, rather than antiferromagnetic. Therefore the anomalous behavior of the fc data below T_{irr} for $x \geqslant 0.48$ cited above most likely arises from ferromagnetic domain effects. In order to investigate this issue, we have carried out additional magnetization measurements on one of the samples with $x=0.65$ (gtk-4-11-4, see Fig. 5) as described in this section. The data reveal evidence for nanoscopic magnetic granularity of ferromagnetic domains, together with frustration and possible "superspin glass" behavior below T_C, as the origin of the unusual behavior of the fc magnetization data for $x \geqslant 0.48$ in Fig. 5.

The $Lu_2V_2O_{6.35}$ sample (gtk-4-11-4) was recovered from a three-year-old XRD microscope slide stored in air. The vaseline and sample on the x-ray slide were washed off using toulene. The susceptibility data between 150 and 300 K in a field of 1 T followed a Curie-Weiss law with $\theta=59.7(4)$ K, $C=1.464(3)$ cm^3 K/mol, and low-field measurements at $H=10$ G gave $T_C=20.1(1)$ K. Comparison of these C and θ values with the previously obtained values for this sample in Table III suggests that the sample slightly oxidized during the three-year storage period in air, although the T_C did not change significantly. The zfc and fc $M(T)$ behaviors at 10 G were essentially the same as seen earlier in Fig. 5, with the two curves bifurcating below an irreversibility temperature $T_{irr} \sim 13$ K.

Detailed hysteresis loops were measured at 1.8 K, as shown in Fig. 8. The magnetization did not saturate up to $H=5.5$ T, in agreement with the above previous results. The virgin magnetization curve obtained after zero-field cooling was S shaped and lay well outside of the subsequently obtained hysteresis loop, with all curves converging by about 2000 Oe. In the returning hysteresis curves, the overall behavior is indicative of a soft ferromagnet with a small coercive field of about 20 Oe. The returning magnetization showed smooth variation with decreasing $|H|$ down to ~50 G below which it dropped sharply in a "goose-necked" (multiplateau) manner with distinct changes at $\sim \pm 20$ Oe. It was found that in the low-field region the magnetization continuously relaxed at a given field value during the time (~30 s) required for measurement at each field value (three scans at ~10 s/scan).

The hysteresis loop data obtained at 15 K, where $T_{irr} < 15\ \text{K} < T_C$, are plotted in Fig. 9. The observed hysteresis, as revealed in the expanded plots in Figs. 9(b) and 9(c), is an artifact of the measurement as follows. First note that the hysteresis loop at 1.8 K in the expanded plot in Fig. 8(c) was traversed in a *counterclockwise* manner, as usual for a ferromagnet below T_{irr}. In contrast, the hysteresis loop measured at 15 K, just above T_{irr} but below T_C, was traversed in a *clockwise* (inverted) direction as seen in the expanded plots in Figs. 9(b) and 9(c). This effect is due to flux that was trapped in the superconducting solenoid upon reducing the solenoid current from large values to zero in a no-overshoot mode, which results in a small trapped field in the sample space in the opposite direction to the originally applied field.[17] This effect was also suggested in a previous study of ferromagnetic granular (Ni,Fe)-SiO_2 films using a Quantum

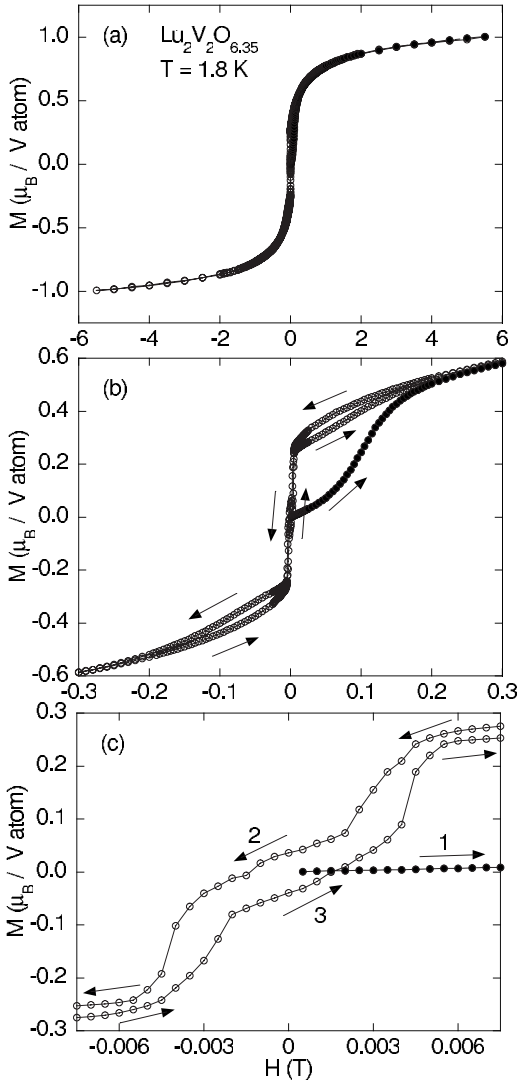

FIG. 8. Magnetization hysteresis measured at 1.8 K for $Lu_2V_2O_{6.35}$ between $H=\pm 5.5$ T after cooling in zero field. (a) The complete loop showing that the sample does not saturate till 5.5 T. [(b),(c)] Detailed view of the low-field region: (b) The initial (virgin) magnetization curve lies well outside the returning curves till they close at 0.2 T. (c) The low coercive field and goose-necked magnetization curve between ±0.005 T are indicative of a collective reversal of strongly correlated spin clusters.

Design SQUID magnetometer.[18] We have confirmed this artifact by observing a hysteresis loop for a high-purity sample of Pd metal provided by Quantum Design, as shown in Fig. 10. The spurious hysteresis loop in Fig. 10 was again traversed in a clockwise direction, and the coercive field in Fig. 10 is about the same as for $Lu_2V_2O_{6.35}$ in Fig. 9. Thus we infer that the actual $M(H)$ behavior of $Lu_2V_2O_{6.35}$ at 15 K is not hysteretic. Correcting for the trapped-flux effect would somewhat increase the remnant magnetization and coercive field for $Lu_2V_2O_{6.35}$ at 1.8 K in Fig. 8.

Zero-field-cooled and field-cooled magnetization $M(T)$ data were obtained on the $Lu_2V_2O_{6.35}$ sample versus temperature at different fixed fields ($H=$ 10, 100, 1000, and 5000 Oe), as shown in Fig. 11. At low fields, both the zfc and fc $M(T)$ showed a significant fall below T_{irr} before lev-

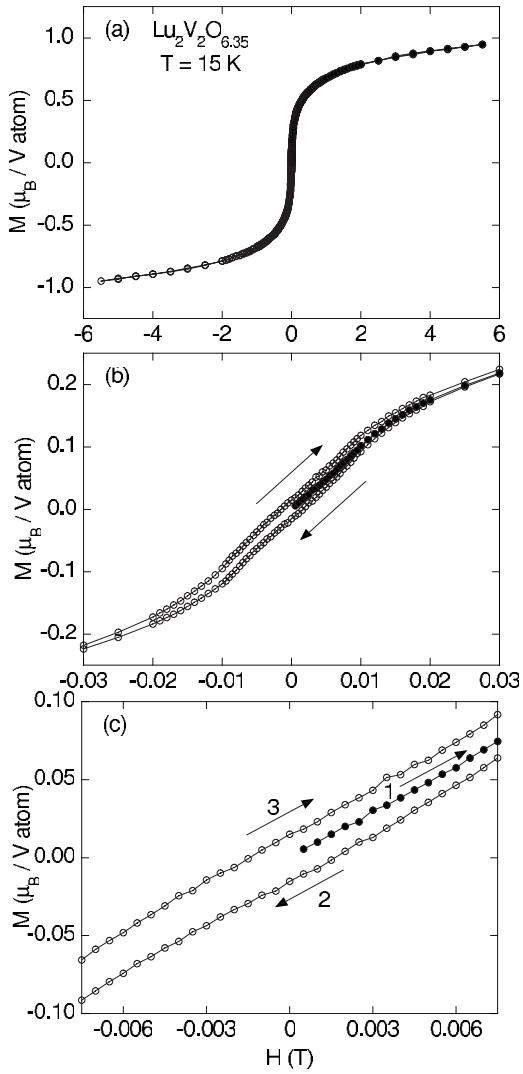

FIG. 9. Magnetization hysteresis measured at a temperature of 15 K for $Lu_2V_2O_{6.35}$ between $H=\pm 5.5$ T after cooling in zero field. (a) The complete loop. (b),(c) Detailed view of the low-field region. The inverted (clockwise) hysteresis loop is an artifact of measurement due to trapped flux in the SQUID magnetometer solenoid as found from similar measurements on a Pd standard, as shown below in Fig. 10.

eling off by ~5 K. With increasing field, the T_{irr} moved down and the peak broadened while the fall in the fc curve was reduced. By 5000 Oe both the zfc and fc $M(T)$ below T_C increase smoothly and monotonically with decreasing temperature.

The anomalous hysteresis and relaxation at 1.8 K (Fig. 8), as well as the variations in zfc and fc $M(T)$ behaviors with temperature and field (Fig. 11) can be qualitatively understood according to the following scenario. We postulate that the crystallographic oxygen sublattice disorder arising from the oxygen vacancies in (crystallographically single-phase) $Lu_2V_2O_{7-x}$ and the associated Lu-V antisite disorder cause the ferromagnetic state below T_C to break up into nanoscopic (~10 nm) ferromagnetic monodomains, to an extent increasing with increasing x. The domains form a dense magnetic nanoparticle system, also termed a "superspin glass," in

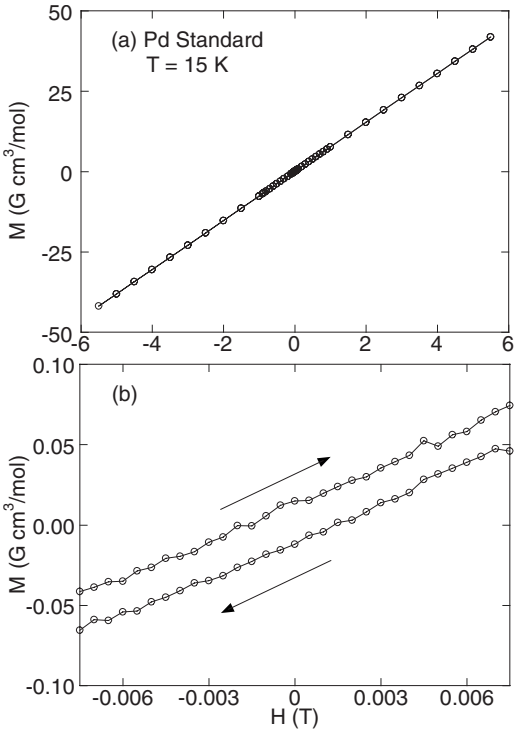

FIG. 10. Magnetization hysteresis measured at $T=15$ K for a Pd standard between $H=\pm 5.5$ T. (a) The complete loop. (b) Detailed view of the low-field region. The apparent inverted hysteresis loop is an artifact of measurement in the SQUID magnetometer (Ref. 18).

which strong dipolar interactions between domains lead to frustration and slow dynamics below the blocking temperature T_{irr}.[19] A characteristic of superspin glass behavior is the fall and subsequent flattening out of the low-field fc $M(T)$ curves below the bifuraction temperature T_{irr}, instead of a monotonic rise to a saturated value as expected for bulk ferromagnets or even superparamagnets. This is clearly observed in our samples as seen in Figs. 5 and 11. Upon cool-

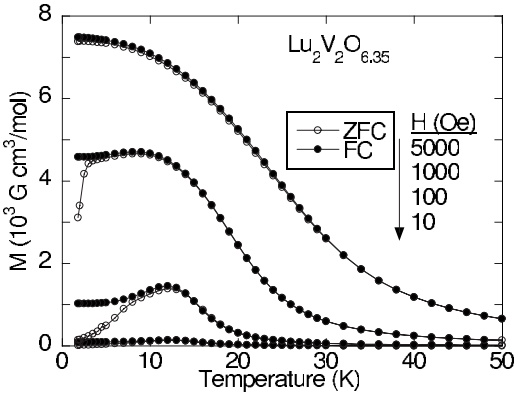

FIG. 11. Zero-field-cooled (zfc) (open circles) and field-cooled (fc) (filled circles) magnetization $M(T)$ data ($H=10$, 100, 1000, and 5000 Oe) for $Lu_2V_2O_{6.35}$. The fall in magnetization below the bifurcation temperature T_{irr} is suppressed as the field is increased, and by 5000 Oe both zfc and fc curves increase monotonically with decreasing T.

ing in zero field below T_{irr}, the monodomains are randomly oriented due to magnetostatic effects and/or dipolar interactions between monodomains. At low fields, this anisotropy energy dominates that due to the Zeeman energy. This leads to a suppression of the net magnetization observed in the zfc virgin $M(H)$ and in both the low-field zfc and fc $M(T)$ data below T_{irr}. For fields greater than 2000 Oe, the Zeeman energy becomes dominant, the domain moments get depinned, and the system changes irreversibly into a coherently oriented ferromagnetic state. Evidently, during the returning part of the hysteresis loop, the oriented cluster moments behave *collectively* and the system switches magnetization direction sharply with a small coercive field. This effect leads to the very unusual situation for a ferromagnet in Fig. 8 that the initial virgin $M(H)$ curve is not bounded by the limiting hysteresis loop between ±5.5 T. The weak relaxation of magnetization in the low-field region is evidently a consequence of the residual competition between the Zeeman energy and the randomizing effect of magnetostatic and/or dipolar interaction effects.

Nanoscopic ferromagnetic domain formation and superspin glass behaviors are also evident in other observations on our samples such as bifurcation between the low-field zfc and fc $M(T)$ behaviors for $T<T_{irr}$ with a decrease of *both* at low temperatures (Fig. 5), lack of saturation up to 5.5 T of the $M(H)$ curves below T_C (Fig. 6), the "goose-neck" (multistep) shape of the hysteresis loop in Fig. 8(c), lack of hysteresis in $M(H)$ for $T_{irr}<T<T_C$ (Fig. 9, see text), and relaxation of the low-field isothermal magnetization below T_{irr} (not explicity plotted here). These behaviors have been observed in other substituted systems such as bulk polycrystalline $La_{1-x}Sr_xCoO_3$ $(x<0.18)$, $La_{0.67-x}A_xCa_{0.33}MnO_3$ $(A=Ce,Y)$, $LaMnO_{3.13}$, $Co_{0.2}Zn_{0.8}Fe_{1.95}Ho_{0.05}O_4$, $La_{1-x}Ca_xMnO_3$, $Tl_2Mn_2O_7$, $Fe_{0.5}Cu_{.5}Cr_2S_4$, $FeCr_2S_4$, amorphous $(Fe_{0.26}Ni_{0.74})_{50}B_{50}$ nanoparticles, and nanocrystalline $Cu_xFe_{3-x}O_4$.[20–28]

IV. SUMMARY AND CONCLUSIONS

We have synthesized and studied the defect pyrochlore series $Lu_2V_2O_{7-x}$ with $x=0.40-0.65$ carried out in an attempt to dope the parent $(x=0)$ ferromagnetic semiconductor $Lu_2V_2O_7$ into the metallic state. The compound $Lu_2V_2O_7$ contains two crystallographically inequivalent oxygen sites denoted as O and O′ sites, and the composition can be written as $Lu_2V_2O_6O'$. For $x\gtrsim 0.5$, significant Lu-V antisite disorder that increases superlinearly with increasing x clearly occurs. This is qualitativbely consistent with our simple structural model for the oxygen vacancies, where oxygen depletion occurs at the O′ site which is tetrahedrally coordinated by Lu in stoichiometric $Lu_2V_2O_6O'$. This model also appears to explain the anomalous nonmonotonic dependence of the lattice parameter on x which initially increases with x for $0<x\lesssim 0.4$, and then decreases for $x\gtrsim 0.4$. We suggest that the Lu_4O' tetrahedra (and the unit cell) first expand as O′ atoms are removed from the centers of the Lu_4 tetrahedra, via elimination of the Lu-O′-Lu bonding within the affected Lu_4 tetrahedra, and then the unit cell subsequently shrinks with further increase in x due to the steadily reduced average oxygen coordination number of the Lu^{+3} cations. Our structural model for the oxygen vacancy position should be testable via future neutron diffraction studies of the O and O′ site occupancies versus x in $Lu_2V_2O_{7-x}$ when samples of sufficient mass are synthesized.

Recent studies on Nb substitution effects, single crystal polarized neutron scattering measurements, and ^{51}V NMR studies indicate that a ferro-orbital ordered state accounts for the simultaneous ferromagnetic and semiconducting behaviors of the undoped $Lu_2V_2O_7$ parent compound.[29–31] The oxygen defect pyrochlore series $Lu_2V_2O_{7-x}$ $(x=0.40-0.65)$ studied here remains ferromagnetic throughout. Unfortunately, the powder nature of the samples prevented us from carrying out conventional electronic transport measurements to determine whether the compounds are insulating or metallic (as $T\rightarrow 0$). The observed Curie constant C in the high-temperature Curie-Weiss behavior of the magnetic susceptibility *increases* rapidly with increasing x, approximately following the mean-field prediction for the mixture of localized $S=1/2$ (V^{+4}) and $S=1$ (V^{+3}) spins dictated by an ionic model for the composition x, suggesting the absence of metallic character of the material over our x range. However, the ferromagnetic ordering temperature T_C and Weiss temperature θ both strongly *decrease* monotonically with increasing x, which is opposite to the behaviors predicted from $C(x)$. Furthermore, the high-field (5.5 T) saturation moment at low temperatures (5 K) is nearly independent of x ($\mu_{sat}\approx 1\mu_B$/V atom, as expected for $S=1/2$) and does not show the expected increase with increasing x, C, and $\langle S\rangle$. These latter three anomalous behaviors suggest that the hole-doped $Lu_2V_2O_{7-x}$ series may actually be metallic, contrary to expectation from the observed $C(x)$, so that both localized ($S=1/2$) and itinerant d electrons may coexist. In that case one would need to explain why the conduction carriers give an apparent Curie-Weiss contribution to the magnetic susceptibility (in addition to that from the localized V^{+4} spins 1/2) that increases with increasing x. The nonlinearity in the inverse susceptibility (Fig. 4) and magnetization versus field data $M(H)$ [Fig. 6(c)] above T_C indicate that short-range interactions persist to temperatures significantly above T_C. These issues will be very interesting to examine further in future experimental and theoretical studies.

We report evidence that the crystallographic disorder present in the reduced ferromagnetic pyrochlore $Lu_2V_2O_{7-x}$ results in nanoscopic magnetic granularity. These ferromagnetic domains with associated dipolar interdomain interactions exhibit superspin glass behaviors below T_C that have also been previously observed in many other magnetically heterogeneous systems on the nanoscale.

ACKNOWLEDGMENT

Work at the Ames Laboratory was supported by the Department of Energy-Basic Energy Sciences under Contract No. DE-AC02-07CH11358.

*Present address: Areté Associates, P.O. Box 6024, Sherman Oaks, CA 91413.

†Permanent address: Department of Physics, Faculty of Natural Sciences, Jamia Millia Islamia, New Delhi 110025, India.

[1] S. Kondo, D. C. Johnston, C. A. Swenson, F. Borsa, A. V. Mahajan, L. L. Miller, T. Gu, A. I. Goldman, M. B. Maple, D. A. Gajewski, E. J. Freeman, N. R. Dilley, R. P. Dickey, J. Merrin, K. Kojima, G. M. Luke, Y. J. Uemura, O. Chmaissem, and J. D. Jorgensen, Phys. Rev. Lett. **78**, 3729 (1997).

[2] For a concise review, see D. C. Johnston, Physica B **281&282**, 21 (2000).

[3] M. A. Subramanian, G. Aravamudan, and G. V. Subba Rao, Prog. Solid State Chem. **15**, 55 (1983).

[4] The A or B sublattice of the pyrochlore structure is itself often called "the pyrochlore structure," a misnomer. The identical sublattice structure also occurs in the B sublattice of the cubic $A[B_2]X_4$ spinel structure and in the B sublattice of the AB_2 C-15 cubic Laves phase structure.

[5] K. Kitayama and T. Katsura, Chem. Lett. **1976**, 815.

[6] G. Bazuev, D. Makarova, V. Oboldin, and G. Shveikin, Dokl. Akad. Nauk SSSR **230**, 869 (1976).

[7] G. V. Bazuev, A. A. Samokhvalov, Yu. N. Morozov, I. I. Matveenko, V. S. Babushkin, T. I. Arbuzova, and G. P. Shveikin, Fiz. Tverd. Tela (S.-Peterburg) **19**, 3274 (1977).

[8] T. Shin-ike, G. Adachi, and J. Shiokawa, Mater. Res. Bull. **12**, 1149 (1977).

[9] J. E. Greedan, Mater. Res. Bull. **14**, 13 (1979).

[10] L. Soderholm and J. E. Greedan, Mater. Res. Bull. **14**, 1449 (1979).

[11] L. Soderholm and J. E. Greedan, Rare Earths in Modern Science and Technology **2**, 393 (1980).

[12] L. Soderholm and J. E. Greedan, Mater. Res. Bull. **17**, 707 (1982).

[13] H. C. Nguyen and J. B. Goodenough, Phys. Rev. B **52**, 324 (1995).

[14] A. Muñoz, J. A. Alonso, M. T. Casais, M. J. Martínez-Lope, J. L. Martínez, and M. T. Fernández-Díaz, J. Magn. Magn. Mater. **272-276**, 2163 (2004).

[15] Rietveld analysis program DBWS-9807A release 27.02.99, ©1998 by R. A. Young, an upgrade of "DBWS-9411—an upgrade of the DBWS programsfor Rietveld Refinement with PC and mainframe computers, R. A. Young, J. Appl. Crystallogr. **28**, 366 (1995)."

[16] W. Kraus and G. Nolze, Powder Cell for Windows, ver. 2.3, 1999.

[17] J. R. O'Brien, Quantum Design, Inc., San Diego, CA (private communication).

[18] X. Yan and Y. Xu, J. Appl. Phys. **79**, 6013 (1996).

[19] M. Sasaki, P. E. Jönsson, H. Takayama, and H. Mamiya, Phys. Rev. B **71**, 104405 (2005).

[20] M. Itoh, I. Natori, S. Kubota, and K. Motoya, J. Phys. Soc. Jpn. **63**, 1486 (1994).

[21] J. Wu, J. W. Lynn, C. J. Glinka, J. Burley, H. Zheng, J. F. Mitchell, and C. Leighton, Phys. Rev. Lett. **94**, 037201 (2005).

[22] J. Wu, H. Zheng, J. F. Mitchell, and C. Leighton, Phys. Rev. B **73**, 020404(R) (2006).

[23] G. Alejandro, L. B. Steren, A. Caneiro, J. Cartes, E. E. Vogel, and P. Vargas, Phys. Rev. B **73**, 054427 (2006).

[24] C. R. Sankar and P. A. Joy, Phys. Rev. B **72**, 132407 (2005).

[25] R. N. Bhowmik, R. Ranganathan, and R. Nagarajan, J. Magn. Magn. Mater. **299**, 327 (2006).

[26] V. Chechersky and A. Nath, Low Temp. Phys. **28**, 562 (2002).

[27] R. D. Zysler, C. A. Ramos, E. De Biasi, H. Romero, A. Ortega, and D. Fiorani, J. Magn. Magn. Mater. **221**, 37 (2000).

[28] S. J. Stewart, R. C. Mercader, R. E. Vandenberghe, G. Cernicchiaro, and R. B. Scorzelli, J. Appl. Phys. **97**, 054304 (2005).

[29] S. Shamoto, N. Nakano, Y. Nozue, and T. Kajitani, J. Phys. Chem. Solids **63**, 1047 (2002).

[30] H. Ichikawa, L. Kano, M. Saitoh, S. Miyahara, N. Furukawa, J. Akimitsu, T. Yokoo, T. Matsumura, M. Takeda, and K. Hirota, J. Phys. Soc. Jpn. **74**, 1020 (2005).

[31] T. Kiyama, T. Shiraoka, M. Itoh, L. Kano, H. Ichikawa, and J. Akimitsu, Phys. Rev. B **73**, 184422 (2006).